AGU PUBLICATIONS

JGR

Journal of Geophysical Research: Atmospheres

RESEARCH ARTICLE
10.1002/2014JD022016

Key Points:
- Southern Hemisphere 2 day wave is subharmonic of diurnal tide
- Southern Hemisphere 2 day wave is anticorrelated with diurnal tide
- Austral summer 2 day wave consistent with parametric subharmonic instability

Correspondence to:
R. L. Walterscheid,
richard.walterscheid@aero.org

Citation:
Walterscheid, R. L., J. H. Hecht, L. J. Gelinas, A. MacKinnon, R. A. Vincent, I. M. Reid, S. J. Franke, Y. Zhao, M. J. Taylor, and P. D. Pautet (2015), Simultaneous observations of the phase-locked 2 day wave at Adelaide, Cerro Pachon, and Darwin, *J. Geophys. Res. Atmos.*, *120*, 1808–1825, doi:10.1002/2014JD022016.

Received 12 MAY 2014
Accepted 20 JAN 2015
Accepted article online 24 JAN 2015
Published online 11 MAR 2015

Simultaneous observations of the phase-locked 2 day wave at Adelaide, Cerro Pachon, and Darwin

R. L. Walterscheid[1], J. H. Hecht[1], L. J. Gelinas[1], A. MacKinnon[2,3], R. A. Vincent[2], I. M. Reid[2], S. J. Franke[4], Y. Zhao[5], M. J. Taylor[5], and P. D. Pautet[5]

[1]Space Science Applications Laboratory, The Aerospace Corporation, Los Angeles, California, USA, [2]School of Chemistry and Physics, University of Adelaide, Adelaide, South Australia, Australia, [3]ATRAD Pty Ltd., Adelaide, South Australia, Australia, [4]Department of Electrical and Computer Engineering, University of Illinois at Urbana-Champaign, Urbana, Illinois, USA, [5]Center for Atmospheric and Space Sciences and Department of Physics, Utah State University, Logan, Utah, USA

Abstract The Southern Hemisphere summer 2 day wave (TDW) is the most dramatic large-scale event of the upper mesosphere. The winds accelerate over ~1 week, may attain $>$ 70 m/s, and are often accompanied by a near disappearance of the diurnal tide and stabilization of the period close to 48 h. We denote this as the phase-locked 2 day wave (PL/TDW). We have examined airglow and meteor radar (MR) wind data from the Andes Lidar Observatory (Cerro Pachon, Chile:30°S, 289.3°E), MR data from Darwin (12.5°S, 131°E) and airglow and medium frequency radar data from the University of Adelaide (34.7°S, 138.6°E) for the behavior of the TDW during the austral summers of 2010, 2012, and 2013. The Cerro Pachon and Adelaide sites are located at similar latitudes separated in longitude by about 120°. We find a remarkable coincidence between the TDW oscillations at Chile and Adelaide for the period January–February 2010. The oscillations are nearly in phase in terms of local time and the minima and maxima repeat at nearly the same local time from cycle to cycle consistent with a phase-locked wave number 3 TDW. Data for this and other years (including Darwin) show that the amplitude of the diurnal tide decreases when the TDW is largest and that this occurs when the period is close to 48 h. These observations support the proposal that the PL/TDW is a subharmonic parametric instability wherein the diurnal tide transfers energy to a TDW that is resonant at nearly 48 h.

1. Introduction

The quasi 2 day wave (TDW), with a typical mean period just above 50 h, is a significant feature of the 80 to 100 km altitude region in both hemispheres. The TDW in both the Northern and Southern Hemispheres appears in the local summer months and achieves maximum amplitude after the summer solstice. Despite the similarities between the hemispheres, there are important differences. The TDW in the southern summer is primarily a zonal wave number 3 feature, whereas in the northern summer it is often a mix of wave numbers 2–4 [*Tunbridge et al.*, 2011]. In the Northern Hemisphere the period is 50 h or longer [e.g., *Muller and Nelson*, 1978; *Harris and Vincent*, 1993], wave growth is rather gradual, and often persists near its maximum amplitude for 1 or 2 months. In contrast, wave growth is rapid for the Southern Hemisphere January wave event and is more pulselike. In addition, the period is often indistinguishable from 48 h (as well as this can be ascertained by inspection), with strong evidence that it is phase locked in local time [*Craig and Elford*, 1981; *Poole*, 1990; *Harris and Vincent*, 1993; *Harris*, 1994], with a given phase of the wave (time of maximum northward wind, say) occurring at the same local time for successive cycles. The same phase repeats from year to year, although the actual days of northward flow during one year versus another do not appear to be related [*Craig and Elford*, 1981; *Harris*, 1994]. We refer to this wave as the phase-locked 2 day wave (PL/TDW).

The PL/TDW scenario is exemplified by its behavior at Christmas Island (1°N) and is described as follows [see *Walterscheid and Vincent*, 1996, Figure 1]. In early January the 2 day wave exhibits meridional wind amplitudes of about 10 m s^{-1} and a period somewhat greater than 50 h. Sometime in mid-January the phase coming from a complex deconvolution of the data begins to stabilize indicating that TDW is approaching a period of 48 h; while this occurs the winds accelerate, achieving magnitudes of a few tens of meters per second or greater over a period of about a week. The peak winds occur when the phase has become nearly constant in time indicating a period very close to 48 h. An essential feature of the PL/TDW is the anticorrelation between the strength of the TDW and diurnal tide [*Walterscheid and Vincent*, 1996; *McCormack et al.*, 2010; *Hecht et al.*, 2010]. Before the

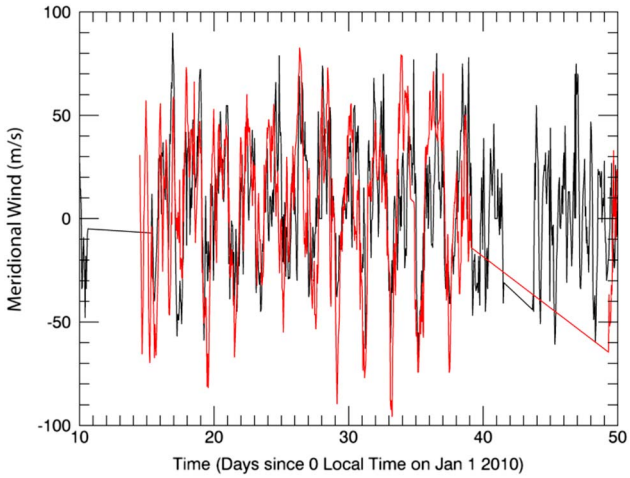

Figure 1. Meridional wind data for 88 km from Buckland Park (black) and the Andes Lidar Observatory (red) versus day of year for a segment in January and February of 2010 where there was substantial overlap. The data are overlaid so that time is expressed in each location's respective local time.

onset of the PL/TDW, the diurnal tide has amplitudes that resemble typical seasonal values, but as the 2 day wave accelerates, amplitudes greatly diminish, with the virtual disappearance of the diurnal tide in some cases. As the PL/TDW abates the diurnal tide reappears, often with preevent amplitudes.

A well-known observation is that an oscillating system will oscillate at a natural frequency if a parameter of the system is made to oscillate at a multiple of the natural frequency; the excitation mechanism being parametric subharmonic excitation [*Minorsky*, 1982]. *Walterscheid and Vincent* [1996] proposed that the PL/TDW is excited by a parametric subharmonic instability (PSI) with a transfer of energy from the tides to a TDW that has been tuned to a subharmonic frequency of the tides [*Ripa*, 1981; *Yeh and Liu*, 1981; *LeBlond and Mysak*, 1978; *McEwan and Robinson*, 1975]. This theory implies an anticorrelation between the TDW and the tides when the TDW is close to phase locked. This behavior has previously been seen in ground-based data [*Hecht et al.*, 2010] and data derived from an assimilation model [*McCormack et al.*, 2010].

Plumb [1983] has argued that the mesospheric solstitial 2 day wave is a baroclinic instability of the summertime easterlies. A one-dimensional stability analysis shows an instability with about the correct growth rate, zonal wave number, and phase speed (period) assuming a basic wind profile that resembles those typically observed. The PSI mechanism provides an explanation for the rapid acceleration of a preexisting TDW as the period stabilizes at nearly 48 h and for the marked anticorrelation with the diurnal tide. *McCormack et al.* [2010] examined the 2 day wave for 2 years, one in which the TDW was phase locked and one in which it was not. They analyzed Navy Operational Global Atmospheric Prediction System (NOGAPS) reanalysis data for altitudes up to about 96 km for each year and found the behavior of the TDW vis-à-vis the diurnal tide was much different depending on whether the TDW was phase locked, the tide being anticorrelated with the TDW when it was, otherwise not. A product wave (diurnal westward $s = 6$ tide or DW6) that mediates the interaction between the TDW and the diurnal migrating tide during phase-locking events was present with large amplitude during the PL/TDW event but not the non-PL/TDW event. Moreover, the acceleration of the winds for the PL/TDW event was far more rapid and the amplitudes attained far greater than for the non-PL/TDW event.

We note that other studies [e.g., *Limpasuvan and Wu*, 2009] show that an $s = 2$ TDW may be observed during periods when the austral summer $s = 3$ TDW undergoes rapid growth. This is not a product of sum and difference interactions between the diurnal migrating tide and a TDW. Parametric interactions involving nonmigrating tides are possible (e.g., the eastward $s = 1$ diurnal tide), but other yet unknown interactions may also be involved.

The TDW has been observed using space-based temperature data (e.g., data from the Sounding of the Atmosphere using Broadband Emission Radiometry (SABER) instrument on the TIMED satellite and the Microwave Limb Sounder (MLS) on the Upper Air Research Satellite [*Limpasuvan and Wu*, 2009; *Azeem et al.*, 2001]). Aliasing spectra indicate that ~10 days is required to characterize a TDW from slowly precessing satellites and that the aliasing bandwidth for the TDW for a 1 week period is several hours [*Gu et al.*, 2013; I. Azeem, ASTRA, personal communication, 2014].

An analysis of MLS ozone and temperature data for January 1993 show a Southern Hemisphere zonal wave number 3 ($s = 3$) TDW with a period that was indistinguishable from 48 h [*Azeem and Palo*, 2000; *Azeem et al.*, 2001]. Data from the same instrument for 2005 austral summer show an "anomalous" Southern Hemisphere TDW with a period for January that was indistinguishable from 48 h. Data for 2006 showed significantly longer periods. Ground-based data radar wind data for the same period, however, showed a strong TDW with

phase locking (similar to that seen in Figure 1) [*McCormack et al*., 2010]. A recent climatological analysis of TIMED/SABER data for the austral summers of 2002–2006 gave an average period of 51 h for individual spectra with 1 month windows [*Huang et al*., 2013]. These data are weighted toward nonphase-locked events and indicate that TDW disturbances in mid-January with periods close to 48 h, or somewhat less, are transient events and are not representative of prevailing conditions over the averaging period. Another recent study based on TIMED SABER temperature and TIMED Doppler Interferometer wind data analyzed over shorter time intervals (1 week) for 2006 showed significant enhancement of the TDW in January with periods closer to the climatological value than to phase-locked values [*Gu et al*., 2013]. However, as mentioned, the aliasing spectrum for a 1 week period was rather broad, and a ground-based study with much better time resolution gave periods very close to 48 h [*McCormack et al*., 2010; *Hecht et al*., 2010].

This study is a follow up to the study of ground-based data [*Hecht et al*., 2010]. That study used radar and airglow data from two sites in Australia: Buckland Park near Adelaide and Alice Springs. This study expands significantly on the coverage to include a much larger range of longitudes and latitudes. We analyze radar measurements of winds and airglow measurements of temperature and brightness from instruments sited at the Andes Lidar Observatory (ALO) (Cerro Pachon, Chile) and Buckland Park (BP). In addition we analyze radar wind data from Darwin, Australia.

Ground-based radar data offer the ability to simultaneously retrieve variations due to the 2 day wave and tides, an essential requirement for assessing unique aspects of PL/TDW dynamics. This cannot be done with data from slowly precessing satellites, such as the Thermosphere Ionosphere Mesosphere Energetics and Dynamics (TIMED) satellite. Ground-based data (especially hourly radar data) allows much better frequency determination and time localization. We use wavelet methods to give good localization and Lomb-Scargle methods to, first, analyze unevenly sampled airglow data and, second, to provide better spectral resolution. Our temporal resolution varies from a few to 6 days with good spectral resolution (2 hours or better). Data from widely separated Southern Hemisphere sites allows us to remove ambiguities relating to the identification of oscillations associated with observed TDW periodicities and allows us to obtain information on the spatial coherence and scale of TDW events over the lifetimes of these events.

In the remainder of the paper we describe the data, present the analysis methodology, give the results, discuss the results, and present the main findings of the work, namely, that the strongest TDW oscillations tend to occur when the period is very close to 48 h (phase locked) and that there is an anticorrelation between the strength of the TDW and the diurnal tide.

2. Data

The data sources are meteor and medium frequency (MF) radar measuring winds in the upper mesosphere and lower thermosphere (covering the altitude range ~80–100 km) and airglow instruments measuring airglow intensity and rotational temperature for OH Meinel emissions in this region. Wind data are from a medium frequency radar at BP and meteor radars at the ALO and Darwin. Airglow temperature and intensity data are from airglow imagers at BP and ALO. Data are from austral summer months for the period December 2009 to February 2013. The primary reliance was on radar data when available, although data availability, coverage, or continuity limited the analysis to a subset of these data sources in some years. These data are hourly and cover both daytime and nighttime hours.

When radar data were available for both ALO and BP the airglow brightness data from those sites were not used. Because brightness data are an indirect measure of the underlying dynamics, they can show large sometimes irregular variations not reflected in the airglow temperature data. In addition, the brightness data are subject to the complexities of the chemical, dynamical, and physical processes that produce the volume emission rate from the underlying wave properties (temperature, density, transport, and line of sight cancelation) [*Walterscheid et al*., 1987; *Hickey et al*., 1992; *Schubert et al*., 1991]. Therefore, these data were not used when airglow temperature data were available. The data used in the study are summarized in Table 1.

2.1. Buckland Park (34.9°S 138.6°E)

The Buckland Park (BP) observational facility is located 35 km north of Adelaide. The Space and Atmospheric Physics Group of the University of Adelaide School of Chemistry and Physics operates a medium frequency (MF) wind radar at this facility. In addition the facility hosts an airglow imager from The Aerospace Corporation.

Table 1. Mesospheric Temperature Mapper (MTM), Aerospace Nightglow Imager (ANI), Medium Frequency Radar (MFR), Meteor Radar (MR), Airglow Brightness (*B*), and Airglow Temperature (*T*)

Summer Season[a]	Site	Instruments	Measurement
2010	ALO	MR	Winds
	BP	MFR	Winds
2011	Data not available or too sparse to analyze		
2012	ALO	MTM	*T*
		MR	Winds
	BP	ANI	*T*
		MFR	Winds
	Darwin	MR	Winds
2013	ALO	MTM	*B*
		MR	*T*
			Winds
	Darwin	MR	Winds

[a]Data may include December of the previous year.

2.1.1. MF Radar

The MF radar located at Buckland Park operates at a frequency of 1.98 MHz and measures winds using the spaced antenna technique in the 60–98 km range by day and in the 80–98 km range by night. Measurements are made every 2 min at 2 km height intervals. Further details about the system and techniques used may be found in the work by *Reid et al*. [1995] and by *Holdsworth and Reid* [2004].

2.1.2. Airglow Imager

The airglow instrument at BP is a modified version of The Aerospace Corporation's charge-coupled device (CCD) nightglow camera which was originally described by *Hecht et al*. [1994] and additionally by *Hecht et al*. [2004] and *Hecht et al*. [2010]. The imager uses a 1536 by 1024 Kodak CCD chip. The pixels are binned 8×8, resulting in images having 192×128 pixels. The angular field of view is 69° by 46° giving a spatial field of view of approximately 122×75 km at 90 km altitude. This instrument obtains images of the OH Meinel (6,2) (hereinafter OHM) and O_2 Atmospheric (0,1) band (hereinafter O2A) band emissions. A sequence of five images is obtained, each at 1 min integration, through separate narrow passband filters. Two of the filters cover two different rotational lines of OHM, two filters measure different portions of O2A, and one monitors the background sky and has almost no airglow emission in its passband. The latter is used to correct the airglow images for background skylight. These data are used to obtain images of the OHM and O2A airglow suitable for determining the band intensity and rotational temperature of the OHM and O2A emissions [*Hecht et al*., 1997, 2001]. For this work we discuss the OHM intensities and temperatures as determined using the techniques described by *Gelinas et al*. [2008].

2.2. Andes Lidar Observatory (Cerro Pachon; 30.3°S, 250.7°E)

The Andes Lidar Observatory (ALO) located at Cerro Pachon in northern Chile began coordinated optical and radar observations in August and September 2009. Instrument capabilities used in the study are the University of Illinois, Urbana-Champaign (UIUC) Meteor Radar, Utah State University (USU) Mesospheric Temperature Mapper, and The Aerospace Corporation's Nightglow Imager.

2.2.1. Meteor Radar

The UIUC Meteor Radar (MR) operates at 40.92 MHz. A single two-element Yagi antenna directed toward the zenith is used to illuminate meteor trails. Meteor trail reflections are coherently detected on five two-element Yagi antennas oriented along two orthogonal baselines, with one antenna in the center of the array common to both baselines. On each baseline, the outer antennas are separated from the center antenna by 1.5 and 2.0 wavelengths. This configuration minimizes antenna coupling, provides enough redundancy to unambiguously determine the azimuth and elevation of most echoes, and provides excellent angular resolution for position determination. The standard format data sets used in this analysis provide hourly winds in the altitude range of 80–100 km, sampled every 1 km. The altitude resolution of these estimates is determined by a triangular weighting function with half-width of 3 km and base width of 6 km. This instrument is essentially identical to the instrument described in the study of *Franke et al*. [2005].

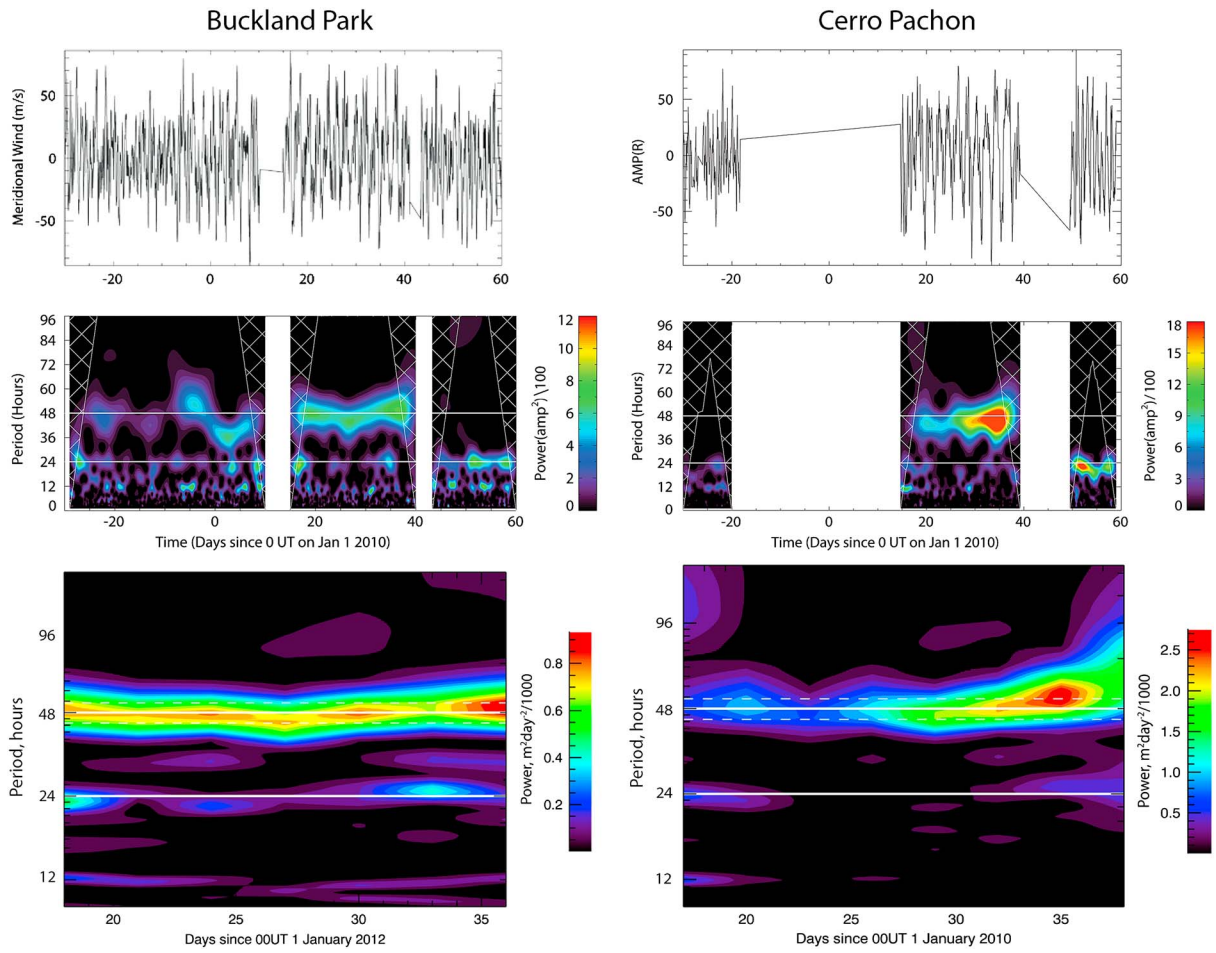

Figure 2. Meridional winds at 88 km from (left) Buckland Park and (right) ALO for the summer months of (top) 2009–2010 and (middle) the corresponding wavelet power and (bottom) Lomb-Scargle power plotted as a function of time (days since 00 UT on 1 January 2010) and wave period. The solid horizontal white lines in the wavelet and Lomb-Scargle plots are for periods of 24 and 48 h. Dashed lines on the Lomb-Scargle plot indicate periods of 44 and 52 h. Dashed lines on the Lomb-Scargle plot indicate periods of 44 and 52 h. The crosshatching on the wavelet plots indicates the cone of influence for edge effects.

2.2.2. Mesospheric Temperature Mapper

The USU Mesospheric Temperature Mapper (MTM) is a mobile CCD imager developed to investigate mesospheric temperature and wave-induced variability and that has operated at several middle- and low-latitude research stations since its construction in 1996. In particular, the MTM operated for a 5 year period at Maui, Hawaii during the Maui-MALT campaign (October 2001 to December 2005) was subsequently deployed at ALO in August 2009 for long-term OH and O_2 temperature and relative band intensity measurements over the Andes.

The MTM measures the hydroxyl OH Meinel nightglow in the (6,2) rotational band and the O_2 (0,1) molecular oxygen band, both in the near infrared. The OH rotational temperature is derived from the intensity ratio of the P1(4)/P1(2) lines within the (6,2) rotational band. Based on typical OH and O_2 emission levels measured at Maui, the precisions of the measurements were determined to be $<$0.5% (in 1 min) for the individual line emission intensities, and $<$1–2 K (in 3 min) for the derived OH and O_2 rotational temperatures. A previous comparison of the MTM OH rotational temperatures with other well-calibrated instruments (a Fourier transform infrared spectrometer and Na temperature lidars) has shown that our nightly mean temperatures, referenced to the 87 km lidar temperatures, are accurate to about ±5 K [*Pendleton et al.*, 2000; *Zhao et al.*, 2005]. Further details of the MTM data reduction and analysis method are given in *Pendleton et al.* [2000] and *Taylor et al.* [1999, 2001].

The MTM has a 90° circular field of view which corresponds to a region of about 150 km in diameter at ~90 km. The image data format are 1024 × 1024 pixels, and are binned 8 × 8 to produce a final resolution of 128 × 128 pixels.

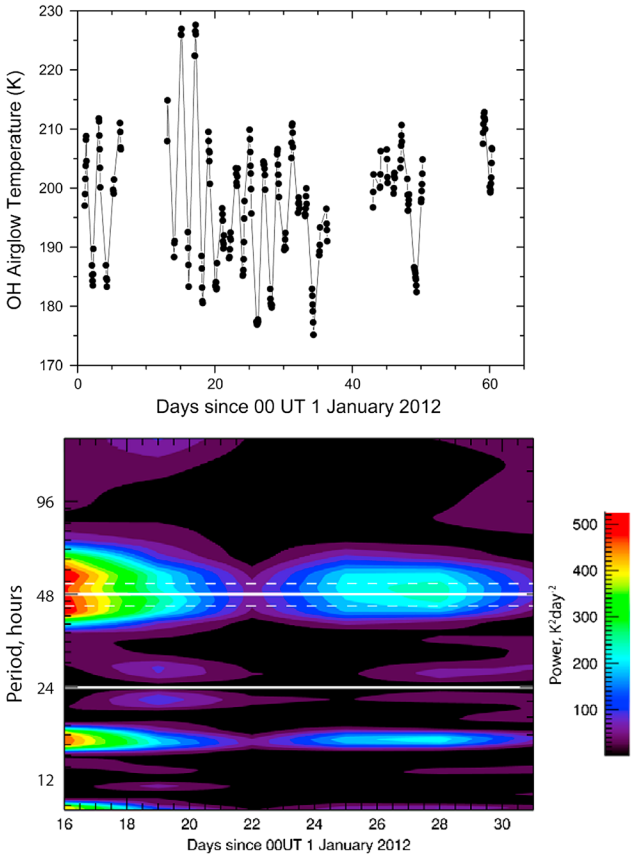

Figure 3. (top) OH temperature data for ALO for a 15 day period in January 2012 and (bottom) the corresponding Lomb-Scargle power versus days since 00 UT on 1 January 2012 and period (days). The horizontal solid lines are for periods of 1 and 2 days. The dashed lines denote 44 and 52 h.

This results in a spatial resolution of 0.6° × 0.6° which corresponds to a "superpixel" footprint of 0.9 km × 0.9 km at upper mesospheric heights. The OH $P_1(2)$ and $P_1(4)$ doublet lines are located at 840.0 nm and 846.5 nm, respectively. The O_2 emission spectrum is sampled at 866.0 nm and 868.0 nm. To monitor sky conditions and measure any background contribution a separate background measurement is made at 857.0 nm. Exposures for each emission sampled are typically 60 s, with about 4 s between each measurement. Measurements are made sequentially resulting in a cyclic determination of temperature for OH and O_2 with a periodicity of about 5 min for each emission. Occasionally, a dark image is also taken to monitor the camera diagnostics. In November 2011, the MTM operation was altered to a high cadence mode using the OH (6,2) band only and 30 s integration time with 2 min cycle time. The MTM operates automatically each night for solar depression angle > 9° and with a ~6 day gap with no measurements during the full moon period.

2.2.3. Aerospace Nightglow Imager

The Aerospace Corporation's near-IR camera (ANI) is described in detail in *Hecht et al.* [2005] for its operation during Maui-MALT. There have only been a few changes for its operation at ALO. The camera has a wide-angle lens with a 256 × 256 HgCdTe detector array to provide images over an ~73 × 73° region of the sky. In an image, 128 pixels across the center is approximately equal to 40°, or 61 km, at 85 km altitude. The array consists of four 128 × 128 quadrants each with their own readout circuitry. A new detector was purchased prior to installation at ALO so that all four quadrants are now operational. A fixed open filter position is used allowing a spectral range (1.55–1.7 μm) determined by the internal filters to be imaged. This spectral range is dominated by the OH Meinel airglow and because the OH Meinel (4,2) band brightness is almost 100 kRy, the signal to noise (S/N) for a 1 s integration is over 200:1.

2.3. Darwin (12.5°S, 131°E)

2.3.1. Meteor Radar

The Darwin meteor radar is a 7.5 kW peak power solid state system with five receive channels. Its antenna system is composed of a single crossed Yagi-transmitting antenna and a receive array of five crossed Yagi antennas which are arranged to form two perpendicular interferometer baselines. It operates at 33 MHz and typically detects 10,000 to 16,000 meteors per day. It provides wind measurement of the winds in the 70–110 km height region. This radar was operated at BP prior to being relocated to Darwin and is fully described by *Holdsworth et al.* [2004].

3. Data Analysis

To analyze the frequency content of the data, we use wavelet and Lomb-Scargle analyses. The wavelets perform better in terms of time localization, and the Lomb-Scargle analysis is better adapted for irregularly spaced data. In addition, we adopt a scheme for the Lomb-Scargle analysis (6 day windows) that allows good

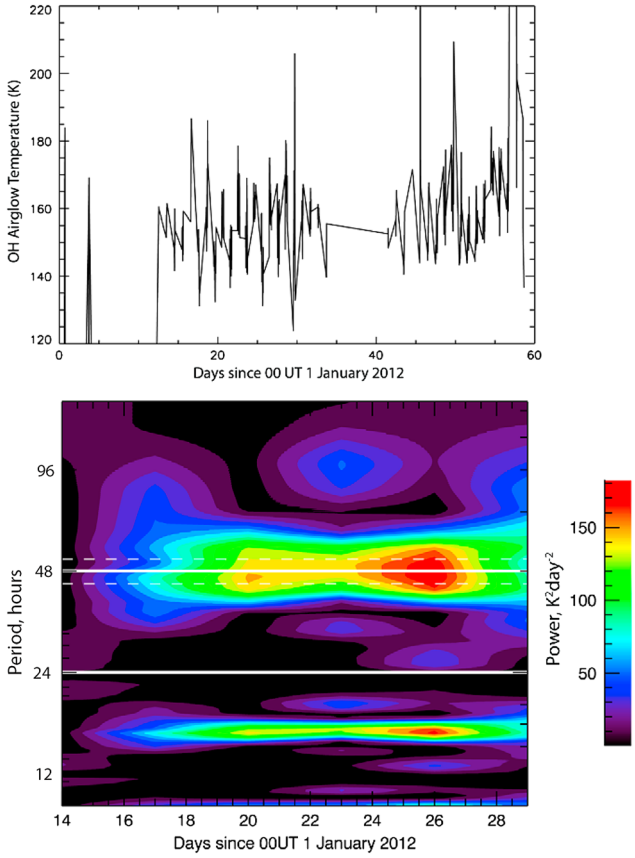

Figure 4. Same as Figure 3 but for BP.

spectral definition. This means that we cannot apply a Lomb Scargle analysis where data segments are too short. The Lomb-Scargle analyses focus on fairly long data segments where significant TDW activity occurs.

3.1. Wavelet Analysis

Our wavelet analysis follows *Torrance and Compo* [1998]. A Morlet wavelet was chosen. To check the spectral separation, we input a fixed-period wave and looked for power in the four band passes that are used to interpret the TDW: The TDW (40 to 60 h), the diurnal tide (20 to 30 h), the semidiurnal tide (11 to 13 h), and the 16 h wave (15 to 17 h). Except for the 16 h bandpass there was typically $\ll 1\%$ leakage of power. Both the diurnal and semidiurnal band passes leaked about 2 to 3% energy into the 16 h bandpass. The reconstructed time series was generally within 1–2% of the original time series. To apply the analysis to irregularly spaced airglow data, we interpolate to evenly spaced points every hour to simulate the temporal resolution of the radar data. Note that the wavelet power in the figures is the wavelet power from the Morlet wavelet divided by the wavelet time scale (approximately equal to the period). This normalizes the power across all periods so that to within a constant factor the variance of a feature is equal to the power integrated across the feature. This normalization gives similar wavelet and Lomb-Scargle amplitudes for features that are fairly narrow band in both analyses. Wavelet results are not calculated for significant (more than 1 day) data gaps (see for example Figure 8).

The region significantly affected by edge effects (the cone of influence) for a Morlet wavelet is about twice the period. Thus, for the diurnal tide the cone ends at about 2 days inward from the edges, while for the TDW it ends at about 4 days from the edges. This is illustrated in Figure 2. In most cases this does not represent a serious limitation on the interpretation of the results. We also note that the cone of influence as defined by *Torrance and Compo* [1998] is where the power diminishes by e^{-2} from the edges. Thus, the edge of the cone is not absolute; there is still some significance even within the cone. We note that the Lomb-Scargle analysis does not suffer from boundary effects and we can use it to assess whether or not a feature in the cone of influence is affected by edge effects to a significant degree.

3.2. Lomb-Scargle Analysis

An alternative method for spectrally analyzing unequally spaced data is the Lomb-Scargle analysis [*Press and Rybicki*, 1989]. We apply the Lomb-Scargle method following the approach used in Short Time Fourier Analysis: A segment of data is analyzed by applying a time window of fixed length τ [*Jacobsen and Lyons*, 2003; *Allen*, 1977; *Walterscheid and Sivjee*, 1996]. The time window is then shifted by a fixed amount $\Delta\tau$ and another segment of duration τ is analyzed. This is carried on until the time interval of interest is covered. The results of analyzing each data segment are applied to the center of the segment to give the time evolution of the spectral content. We chose $\tau = 6$ days and $\Delta\tau = 3$ days. We normalize the results so that the result of analyzing a simple sinusoid defined on equally spaced data gives the squared amplitude of the sinusoid. This gives a good correspondence between the calculated amplitude and the amplitude inferred from an inspection of the time series for the data sets we use.

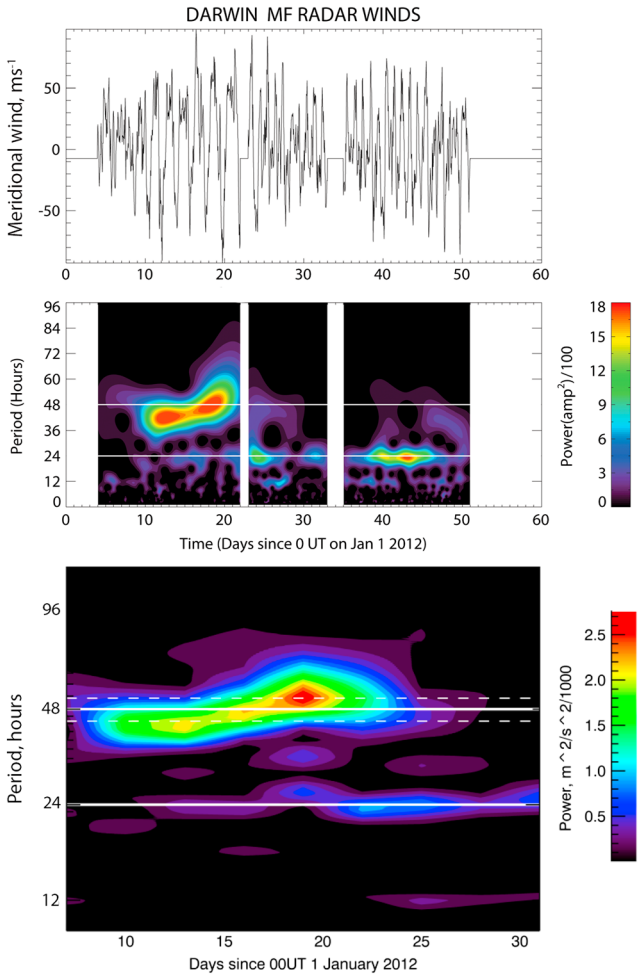

Figure 5. (top) Meridional winds at Darwin for 88 km for January and February of 2012 and (middle) the corresponding wavelet power and (bottom) Lomb-Scargle power plotted as a function of time (days since 00 UT on 1 January 2010) and wave period. The horizontal white lines in the wavelet plot are for periods of 24 and 48 h. The horizontal solid lines in the Lomb-Scargle plot are for periods of 1 and 2 days. The dashed lines denote 44 and 52 h. The Lomb-Scargle power has been normalized to indicate the square of wave amplitude for a pure sinusoid.

4. Results

In this section we present wind and airglow data and give results of the wavelet and Lomb-Scargle analyses for three austral summer seasons: 2010, 2012, and 2013 (insufficient data are available for a 2011 study).

4.1. Summer 2010

Figure 1 shows meridional wind data for 88 km from BP (black) and ALO (red) versus day of year for a segment in January and February of 2010 where there was substantial overlap (days 15–39). The TDW is a fairly deep oscillation peaking in the upper mesosphere and data from 88 km should be more or less representative of this region [*McCormack et al.*, 2010]. The data are overlaid so that time is expressed in each location's respective local time. A strong 2 day wave is evident with an amplitude of ~50 m/s or greater. The data were taken approximately 120° of longitude apart and show a remarkable coincidence. This indicates that the oscillation is strongly dominated by multiples of wave number 3 ($s = 3$). This is almost certainly the westward propagating normal mode with $s = 3$ [*Tunbridge et al.*, 2011]. A close inspection of the data indicates that the maxima and minima over the main part of the overlap region occur at nearly the same local time at both locations indicating that the periods are close to 48 h. The repeatability of the times of data minima and maxima is what is meant by phase locked. Such a wave has the attribute of being a subharmonic of the diurnal tide.

Figure 2 shows meridional wind data from BP and ALO at 88 km altitude for the summer months of 2009–2010 (top) and the corresponding wavelet (middle) and Lomb-Scargle (bottom) analyses. Horizontal solid white lines on the wavelet and Lomb-Scargle plots denote periods of 24 and 48 h. The dashed lines denote periods of 44 and 52 h. An earlier analysis indicated that no significant anticorrelation between the 2 day wave and the diurnal tide occurs when the wave period was as short as 44 h [*Hecht et al.*, 2010]. The cross-hatched areas at the left and right boundaries of individual wavelet plots denotes the region where the wavelet amplitudes may be significantly affected by boundary effects (see discussion in section 3.1).

The data and analysis results for BP are shown on the left. In the segment preceding the data gap from 10 to 15 January the wavelet analysis shows a weak 2 day wave that varies in period meandering between ~40 and 55 h. A mostly weak and episodic diurnal tide is seen during this segment. After the gap ends in mid-January a strong oscillation with a period close to 48 h appears and persists through the interval ending in a second gap commencing on 9 February. During this period the initial appearance of the TDW in the analysis is a fairly narrow band but large amplitude feature with a period very close to 48 h. This spectral feature lasts for about a week. The buildup to the peak value is associated in time with a moderate-amplitude diurnal tide that essentially

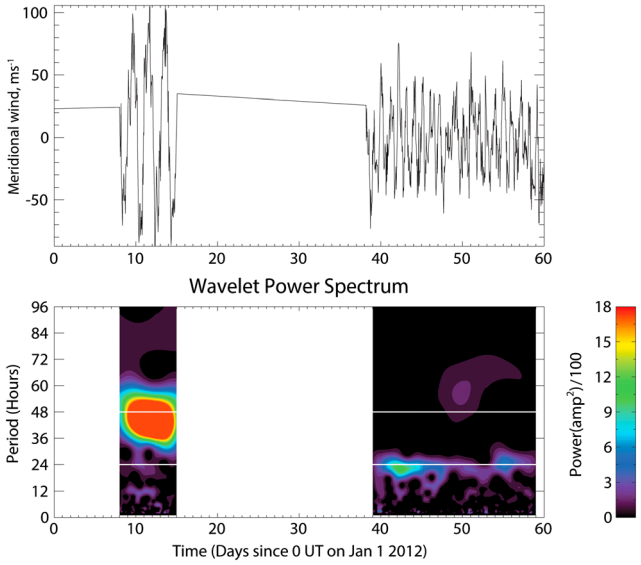

Figure 6. (top) Meridional winds at ALO for 88 km for January and February of 2012 and (bottom) the corresponding wavelet power plotted as a function of time (days since 00 UT on 1 January 2010) and wave period. The horizontal white lines in the wavelet plot correspond to periods of 24 and 48 h.

disappears after the TDW feature attains its peak value. Except for a brief burst with period close to 44 h the TDW continues as a comparatively weak oscillation until the end of the interval when a fairly broadband fairly large-amplitude feature with a central frequency near 50 h appears. It persists until near the commencement of the second gap. A moderate-amplitude diurnal tide is evident as this TDW feature increases toward its peak value and then it essentially disappears. Between the buildup to the TDW peaks at the beginning and end of the data segment, the behavior of the diurnal tide resembles its behavior before the first data gap, mostly weak and episodic. By the time the second data gap ends on about 14 February the 2 day wave has disappeared and the diurnal tide has become stronger and more persistent than either before or while the 2 day wave is strongest and essentially phase locked (the period between 15 January and 10 February).

The Lomb-Scargle analysis covers the central data segment (17 to 36 days) when a moderately strong TDW is evident. The analysis shows a TDW feature that is more or less continuous over the entire segment varying in amplitude between ~20 and 30 m/s. The period varies somewhat but averages close enough to 48 h so that periods departing from 48 h by only a few percent are clearly off the peak power over the main part of the data interval covered. The general features are similar to those discussed in the previous paragraph, but the TDW feature extends over the full segment, indicating that in the wavelet analysis the appearance of onset and termination of the TDW near the beginning and end of the data interval were most likely boundary artifacts. The diurnal tide is comparatively weak over this segment, generally less than ~10 m/s. There are two episodes of increased amplitude where values attain ~20 m/s. The first occurs at the earliest time analyzed day 18 and the other near day 33. For the first the TDW and diurnal amplitudes both diminish, but there is no prior history to indicate whether the TDW had diminished from significantly larger values. For the feature that is wholly contained within the data segment, there is a clear anticorrelation between tidal and TDW amplitudes.

The data and analysis results for ALO are shown on the right. There is a short data segment in mid-December followed by a long data gap ending near 15 January. A second gap occurs over the period from about 10–20 February followed by a short data segment over the remainder of February. The results of the wavelet analysis are similar to those shown in for BP. The data show a TDW oscillation with a period close to 44 h commencing few days after the data gap ending 15 January. The strength of the oscillation grows dramatically toward the end of January and persists until near the end of the data segment when either end effects or the vanishing of the TDW causes the wavelet feature to disappear. The diurnal tide appears weak to nil and is episodic throughout. After the data gap ending about 20 February the 2 day wave has disappeared while a significant diurnal tide has appeared.

The Lomb-Scargle analysis covers the segment containing the TDW feature. The features are similar. The period is close to 48 h until about day 33 when it begins to migrate toward longer periods and broaden spectrally. Initially, it strengthens somewhat (to ~50 m/s), but then rapidly diminishes. It attains a central period of around 2.5 days by the end of the segment. After day 33 the diurnal tide strengthens attaining amplitudes on order of 30 m/s, compared to essentially nil over the preceding 2 weeks or so while a PL/TDW is in existence.

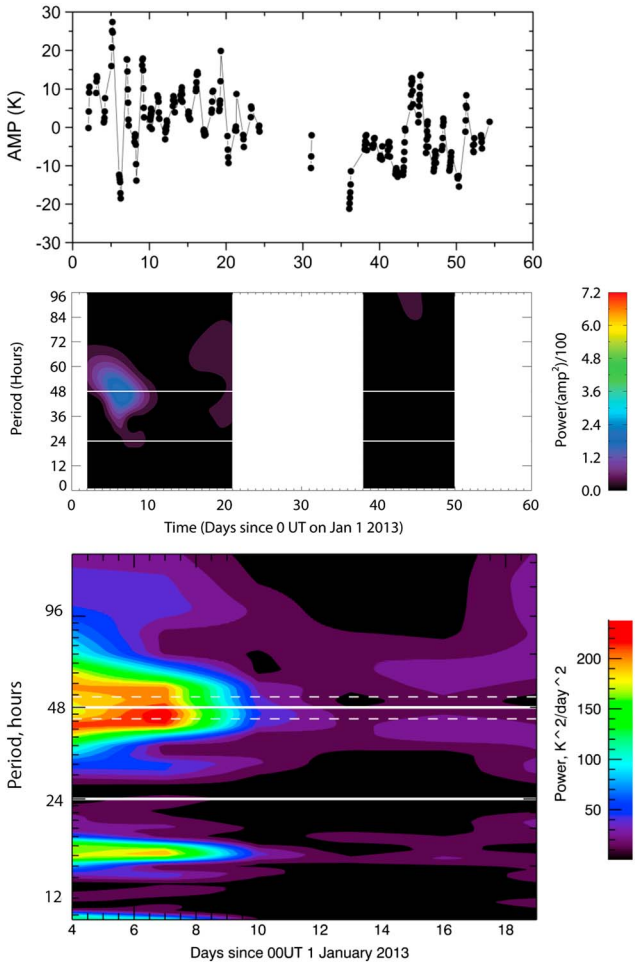

Figure 7. (top) ALO OHM airglow MTM temperature for January–February 2013, (middle) wavelet power, and (bottom) Lomb-Scargle. The horizontal white lines in the wavelet plot correspond to periods of 24 h and 48 h. The horizontal solid lines in the Lomb-Scargle plot are for periods of 1 and 2 days. The dashed lines denote 44 and 52 h. The Lomb-Scargle power has been normalized to indicate the square of wave amplitude for a pure sinusoid.

Note that diminution of the TDW seen in the results of the wavelet analysis near the end of the data segment is by no means an artifact of the cone of influence since the diminishment is also seen in the Lomb-Scargle analysis which does not suffer from edge effects. Thus, hereafter we exclude the cone of influence because it can be misleading and rely on the Lomb-Scargle analysis and the rule of thumb mentioned in section 3.1 (edge effects extend about twice the period inward from the beginning and end of a time segment) to identify edge effects in the wavelet analysis.

4.2. Summer 2012

As mentioned no usable data were available for 2011. During the summer of 2012 airglow data and wind data were available at both ALO and BP. In addition meteor wind data were available from Darwin.

4.2.1. Airglow Data

For the airglow temperature data of this year we rely on a Lomb-Scargle analysis. The localization is not as good as for the wavelet analysis but is ideal for irregularly spaced data with gaps due to nighttime measurements only.

With the irregular time sampling for ALO and BP airglow measurements, tests showed that the Lomb-Scargle analysis reproduced the correct frequency of a pure sinusoid, but produced some artifacts, notably a 16 h spectral feature, most likely an artifact of the simultaneous presence of the TDW and diurnal tide combined with limited local time coverage. Another feature is that while the peak frequency is constant at the input frequency, the amplitude varies significantly as a function of the spacing. The Lomb-Scargle amplitudes can also be sensitive to the phase of the oscillation. An analysis of a 48 h wave form shifted in phase by 45° in successive analyses shows that there is virtually no frequency shift due to the phase shifts, but the ALO sampling for a phase near 135° showed a significant reduction in amplitude. Thus, the inferred amplitudes should be interpreted with caution. Since the airglow data are limited to nighttime hours, the analysis greatly diminishes the diurnal tide and produces a semidiurnal artifact. Thus, the results of the analysis of airglow data have no application to diurnal tides.

Figure 3 shows a Lomb-Scargle analysis (bottom) of OH temperature data from the ALO MTM (top) for a 12 day period in January 2012. The data show a strong 2 day wave (amplitude ~20 K) with a central period very close to 48 h at the onset and another weaker one (amplitude ~15 K) developing about midway into the interval. The appearance of amplitude decay and growth represents real features of the oscillation as a pure 48 h wave does not have similar features when analyzed with the same time sampling. A prominent feature of the analysis is a strong 16 h peak that, as previously mentioned, is most likely an artifact of the sampling.

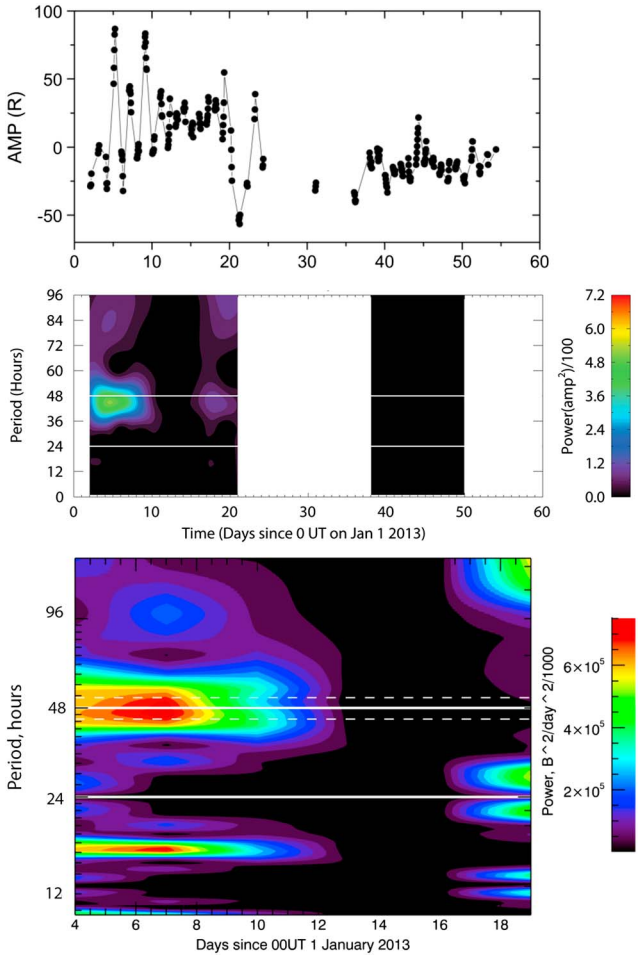

Figure 8. (top) ALO OHM airglow MTM brightness (deviation from average) for January–February 2013 for ALO, (middle) wavelet power, and (bottom) Lomb-Scargle. The horizontal white lines in the wavelet plot correspond to periods of 24 h and 48 h. The horizontal solid lines in the Lomb-Scargle plot are for periods of 1 and 2 days. The dashed lines denote 44 and 52 h. The Lomb-Scargle power has been normalized to indicate the square of wave amplitude for a pure sinusoid.

Figure 4 is similar but for data taken by the airglow imager at BP. Both 48 h features are seen, though the one occurring earlier is somewhat weaker. The putative 16 h artifact is clearly evident.

4.2.2. Wind Data

Figure 5 shows the meridional wind data from Darwin (top) at an altitude of 88 km for data covering days of year 5 to 52 in three segments with brief gaps near days 23 and 35. The wavelet analysis (Figure 5, middle) shows a strong TDW feature appearing around 10 January. The central period is less than 44 h initially, increasing monotonically until it attains a period close to 52 h on about 20 January, after which time end effects are evident. The migration of period occurs in two phases. The initial phase is a slow increase culminating in a period near 44 h. The second phase increases more rapidly. The diurnal tide during the first data segment is rather weak, increasing in amplitude just before and just after the second phase of the TDW feature. The second data segment (days 23–34) shows a weak poorly defined TDW persisting about halfway through the segment. A moderately strong diurnal tide coexists with the TDW and continues through most of the remainder of the segment and on into the third segment, which commences near day 36 (8 February). The diurnal tide strengthens considerably in the middle part of the third segment. A suggestion of a TDW appears after the tide abates.

The main features of the Lomb-Scargle analysis for the first data segment are similar to those of the wavelet analysis. The main difference is that the peak power lies closer to 48 h, especially toward the end of the segment. The peak amplitude of the TDW is close to 55 m/s. The diurnal tide is weak until the central period of the TDW moves somewhat above 48 h. The TDW continues to grow in amplitude for a few days and then decays. The diurnal tide begins to strengthen while the TDW is near its maximum amplitude but is significantly longer than 48 h in period. The diurnal tide reaches its maximum value (~30 m/s) after the TDW has decayed to ~35 m/s. The tide persists with moderate power through most of the remaining part of the segment.

Figure 6 shows the wind data and analysis results for data from ALO for January and February. The data comprise two segments separated by a long data gap. The first segment covers the period from day 8 to day 15. A very strong TDW feature appears which most likely covers the entire segment. It is centered near a period of 46 h, but is very broad, the nonlocalization most likely reflecting the short duration of the segment. A visual inspection shows a very clear TDW signal with a period close to 48 h (three cycles with a total duration of close to 6.0 days). The amplitude of the TDW is ~50 m/s. There is only a hint of a diurnal tide in the wavelet analysis. The second segment commences on day 38 and ends on day 60. There is no feature that

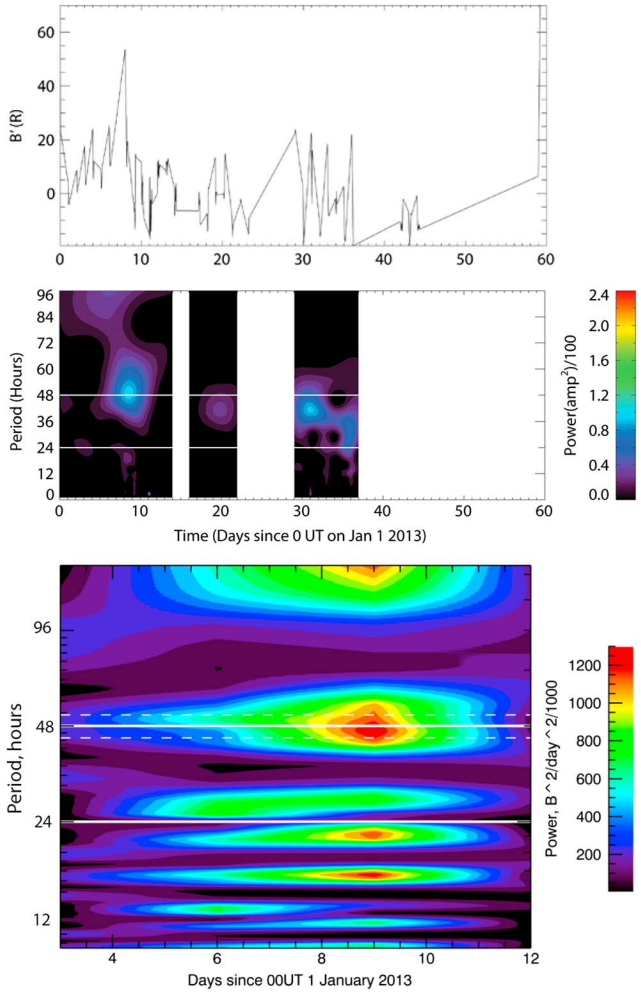

Figure 9. (top) OHM airglow intensity (deviation from average) for January–February 2013 for BP and (middle) wavelet power spectrum. The horizontal lines in the wavelet plot correspond to periods of 24 and 48 h. The horizontal solid lines in the (bottom) Lomb-Scargle plot are for periods of 1 and 2 days. The dashed lines denote 44 and 52 h. The Lomb-Scargle power has been normalized to indicate the square of wave amplitude for a pure sinusoid.

can be associated with the TDW. A moderate diurnal tide is fairly continuous over the first half of the segment, becoming weaker and episodic in the second half.

4.3. Summer 2013

For the summer months of 2013 airglow data were available from both ALO and BP. Radar data were available from Darwin and ALO. Limited temperature data were available from BP but were insufficient for this analysis.

4.3.1. Airglow Data

Figure 7 shows the MTM airglow temperature data from ALO for January and February 2013 and the corresponding wavelet and Lomb-Scargle analyses. The data comprise two segments separated by a long (16 day gap) where the data are too sparse to analyze. The first segment covers the period 1–23 January. The wavelet analysis shows a moderate TDW feature existing at or appearing near the onset of the first segment, as far as this can be determined considering end effects. This feature persists for ~10 days. The feature is relatively broadband with a central frequency of 48 h or slightly less. The Lomb-Scargle analysis for this period shows TDW power peaking in about the same time interval and with the same frequency.

Figure 8 shows the MTM airglow brightness and spectral analyses for the same sampling. The wavelet analysis shows a moderately strong TDW feature in the first segment. The onset is obscured by edge effects in the wavelet analysis, but the Lomb-Scargle analysis suggests that it existed at the start of the segment. This feature persists for ~10 days. It is relatively broadband with a central frequency of ~48 h. The broadband nature is most likely related to the large spikes in the data located near 5 and 9 January. The Lomb-Scargle analysis for this period shows TDW power peaking in about the same time interval and with the same frequency but with better spectral definition and with the peak power is near 48 h.

The wavelet analyses for the second segment, commencing on about 17 February, shows a broadband feature with a central period near 72 h. However, this result is probably an artifact of the spikes that occurred during this period.

Figure 9 shows the airglow brightness data from BP for January and February 2013 and results from a wavelet and Lomb-Scargle analysis. The data are divided into three segments separated by data gaps. The first segment covers the period from 1 to 13 January. The wavelet analysis shows a broadband TDW feature with a central period somewhat greater than 48 h covering most of the second half of the segment. The broadband nature is most likely a result of the large spike occurring around 8 January. The Lomb-Scargle analysis does a much better job of localizing the TDW in frequency space. The central period is very close to

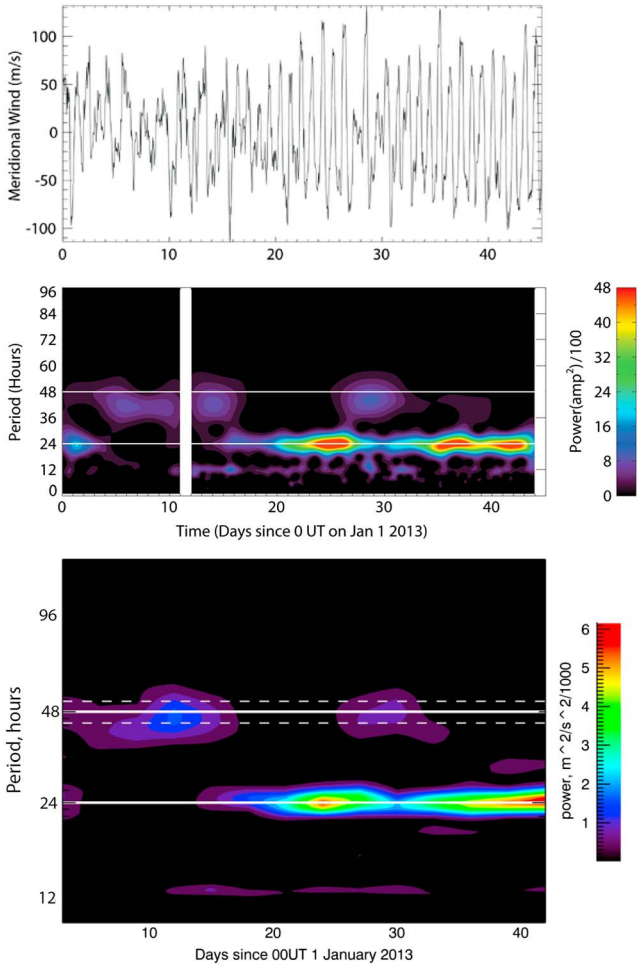

Figure 10. (top) Meridional winds at Darwin for 88 km for January and February of 2013 and (middle) the corresponding wavelet power and (bottom) Lomb-Scargle power plotted as a function of time (days since 00 UT on 1 January 2010) and wave period. The horizontal white lines in the wavelet plot are for periods of 24 and 48 h. The horizontal solid lines in the Lomb-Scargle plot are for periods of 1 and 2 days. The dashed lines denote 44 and 52 h. The Lomb-Scargle power has been normalized to indicate the square of wave amplitude for a pure sinusoid.

48 h. Tests show that the brightness spike makes a significant contribution to the power seen in the various other spectral features. Power from the TDW due to the irregular temporal sampling contributes as well.

The second segment covers a 6 day period commencing on 16 January. It is essentially featureless. The third segment covers the last few days of January and the first week of February. It shows broadband TDW power centered near 42 h. A Lomb-Scargle analysis (not shown) gives a broadband feature that is split, with a distinct minimum close to 48 h. The power is asymmetrically distributed with somewhat greater values below than above 48 h We note that large spikes (excursions) in the airglow brightness preceding a strong TDW event such as seen in the data for ALO and BP (Figures 7–9) are rather common [*Hecht et al.*, 2010].

4.3.2. Wind Data

Figure 10 shows the results of wavelet and Lomb-Scargle analyses of the Darwin meteor radar meridional wind data for January and February of 2013. The data (Figure 10, top) comprise two segments separated by a 1 day data gap commencing on 11 January. The wavelet analysis over the first segment (Figure 10, middle) shows brief episodes of moderate power at the diurnal period and TDW frequencies. The peak in the diurnal tide leads the peak in the TDW by a few days. The localization of the diurnal feature may be an artifact of the nearness to the onset of the period analyzed. The period of the TDW feature is ~40 h. The termination of the TDW feature is only apparent, being an artifact of end effects. As the Lomb-Scargle analysis shows, it continues into the next segment before vanishing near day 17. The second data segment is the longest continuous data segment in our data set. It also contains he strongest and best defined diurnal tide. A strong diurnal tide (peak amplitudes attaining ~70 m/s) commences on about day 21 and weakens considerable by day 27. At the same time a moderate TDW wave appears with a central frequency near 46 h. As the TDW weakens the diurnal tide begins to strengthen. By about day 33, the diurnal tide has returned to amplitudes on the order of those before the appearance of the TDW maximum. A weak TDW with variable period persists until the end of the segment.

The Lomb-Scargle analysis performed over both segments (across the one-day gap) shows similar features. The initial TDW feature has peak amplitudes near 45 m/s and a central period near 46 h. It persists from day 1 to around day 17. During this main part of this period the diurnal tide is essentially nonexistent. As the leading TDW feature weakens the diurnal tide increase in amplitude attaining its peak value near day 24 and weakening thereafter until a minimum is reached near day 30. As the tide diminishes a TDW reappears attaining its peak value (~10 m/s) near where the tide reaches its minimum value. The period of the TDW

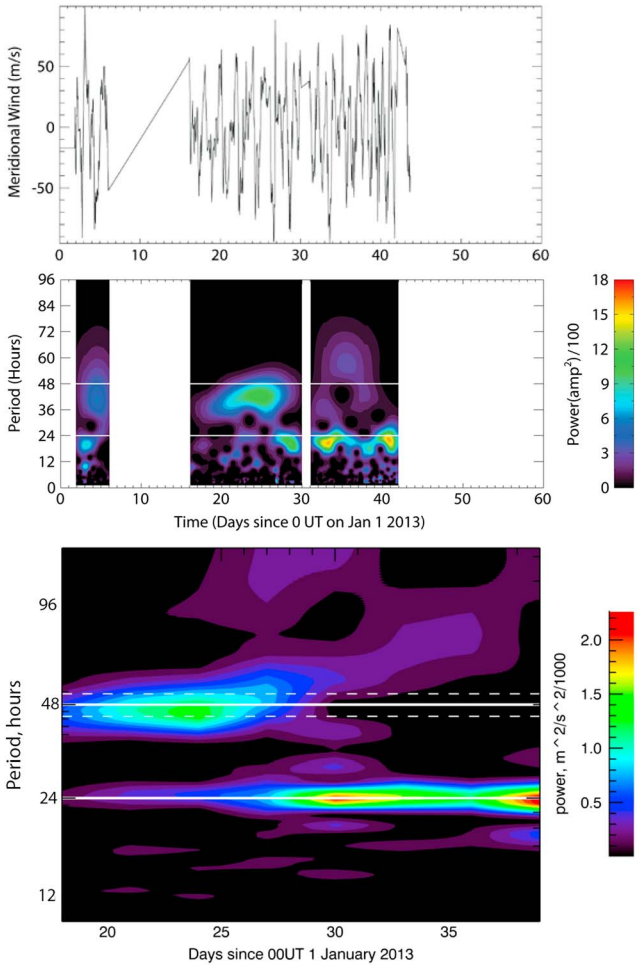

Figure 11. (top) Meridional winds at ALO for 88 km for January and February of 2013 and (middle) the corresponding wavelet power and (bottom) Lomb-Scargle power plotted as a function of time (days since 00 UT on 1 January 2010) and wave period. The horizontal white lines in the wavelet plot are for periods of 24, 44, and 48 h. The horizontal solid lines in the Lomb-Scargle plot are for periods of 1 and 2 days. The dashed lines denote 44 and 52 h. The Lomb-Scargle power has been normalized to indicate the square of wave amplitude for a pure sinusoid.

isclose to 48 h. The TDW essentially vanishes near day 35 and does not reappear. From day 30 to the end of the segment the diurnal tide increases in strength approaching 80 m/s.

Figure 11 shows the results of wavelet and Lomb-Scargle analyses of the ALO meteor radar meridional winds for January and February of 2013. The data comprise three segments. The first is a brief segment of a few days duration separated from the second by a long data gap. The first segment shows a broadband TDW feature and evidence of a diurnal tide. The segment is too brief to draw any meaningful conclusions. The second segment commences on 16 January and ends on 30 January. A moderately strong TDW feature centered in period near 42 h appears around day 21 and persists to around day 27. A moderate diurnal signature appears as the TDW abates. The third segment commences after a 1 day gap. The diurnal tidal feature from the second segment continues into the third and persists to the end of the data coverage. Short burst of moderately amplitudes are seen near days 33 and 41.

A Lomb-Scargle analysis is done for days 16–41 (across the 1 day gap). The TDW feature is found to have a period near 46 h and peak amplitude of ~35 m/s. The period migrates to values above ~52 m/s as it weakens and becomes nearly nonexistent. The diurnal tide is rather weak until the TDW has abated. Diurnal amplitudes increase from their lowest values (~20 m/s) attained while the TDW is increasing in amplitude up to values near 50 m/s after the TDW has migrated to longer periods and substantially disappeared.

Figure 12 shows the results of wavelet and Lomb-Scargle analyses of the BP meteor radar meridional winds for December 2012 and January 2013. There is a large gap that covers the period of time when the TDW event at ALO shown in Figure 11 occurs. A weaker event occurs earlier in January at BP (when a gap occurs in the ALO data). This event begins near the first of January with a period very close to 48 h. At the same time a moderate diurnal tide (~20 m/s) begins to diminish and becomes weak to nonexistent until the TDW feature itself diminishes to very small values. The peak period drifts to values near 44 h before the TDW decays. The TDW feature is coincident with TDW events seen in early January in the MR winds at Darwin (Figure 10) and in the airglow temperature and brightness at ALO (Figures 7 and 8) and airglow brightness BP (Figure 9). In these data the period is closer to 48 h throughout.

5. Discussion

The main goal of the study was to examine the simultaneous behavior of the TDW in the austral summer at two sites at similar latitudes, but widely separated in longitude (BP and ALO) and sites similar longitudes but

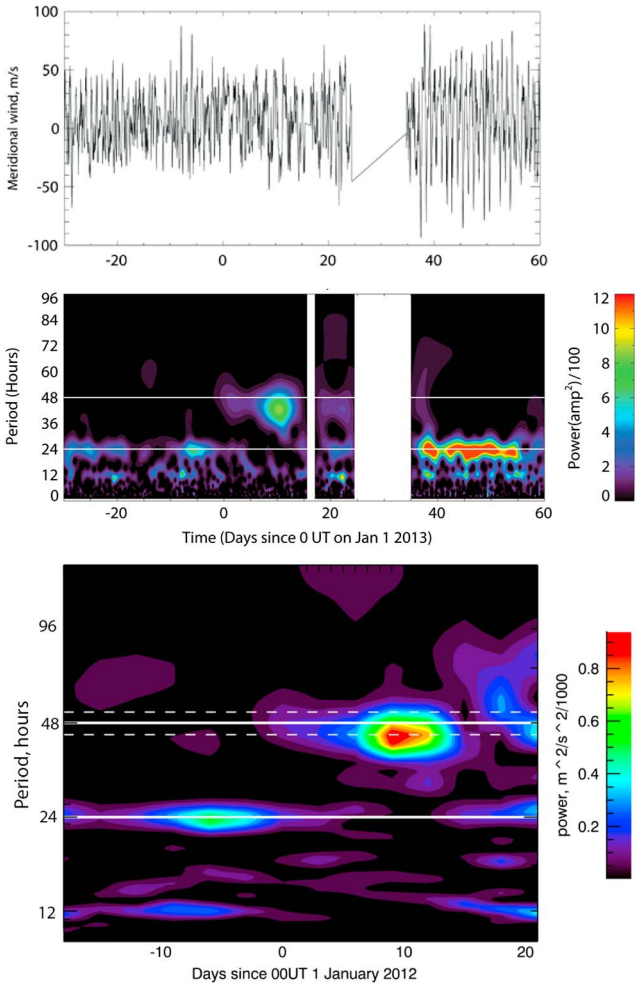

Figure 12. (top) Meridional winds at BP for 88 km for December 2012 and January 2013 and (middle) the corresponding wavelet power and (bottom) Lomb-Scargle power plotted as a function of time (days since 00 UT on 1 January 2010) and wave period. The horizontal white lines in the wavelet plot are for periods of 24, 44, and 48 h. The horizontal solid lines in the Lomb-Scargle plot are for periods of 1 and 2 days. The dashed lines denote 44 and 52 h. The Lomb-Scargle power has been normalized to indicate the square of wave amplitude for a pure sinusoid.

separated in latitude (BP and Darwin). During austral summer the TDW can accelerate to large amplitudes over a period of days and become phase locked so that its period is very close to a subharmonic of the diurnal tide. We denoted this TDW wave as the phase-locked TDW (PL/TDW).

Walterscheid and Vincent [1996] proposed that the rapid acceleration occurred when the TDW normal mode period was tuned to a subharmonic period of the tides. Since the PL/TDW is a subharmonic of the diurnal tide, a parametric subharmonic instability (PSI) interaction between the forced diurnal tides and the normal mode PL/TDW may proceed. In this interaction the TDW derives its energy from the diurnal tide. Evidence of this interaction is an anticorrelation between the tides and the TDW when the TDW period is close to 48 h. Thus, we also examine the behavior of the diurnal tide.

We rely primarily on the radar data since these data are hourly and give coverage for both daytime and nighttime hours. This coverage allows the simultaneous retrieval of the tides and longer-period oscillations. The airglow data are nighttime only and are adequate for periods of 2 days and longer but are not able to reliably represent the tides. We have therefore used airglow data to augment the radar data when the latter are limited or nonexistent.

To analyze the data, we use a combination of wavelet and Lomb-Scargle analysis. Wavelets are best suited for time localization of periodic features with time-varying amplitude. To apply them to unequally spaced data, we interpolate the data to an evenly spaced grid. This may produce artifacts, including undue sensitivity to data spikes. To provide better frequency discrimination (at the expense of localization) and reduce the sensitivity to data spikes, we also use a sliding Lomb-Scargle analysis with a 6 day window. This also provides better accuracy on irregularly spaced data.

The wind data from ALO and BP for January 2010 when overplotted against local time show a remarkable coincidence in terms of the temporal behavior. The variation is dominated by a strong TDW (amplitude exceeding 50 m/s at the ALO) with maxima and minima occurring at nearly the same local time. In addition, the extrema occur at nearly the same local time through ~8 cycles. This behavior characterizes the PL/TDW. Since ALO and BP are separated by approximately 120° of longitude, this behavior is consistent with an essentially pure zonal wave number 3 ($s = 3$).

This PL/TDW behavior is confirmed by wavelet and Lomb-Scargle analyses for this and subsequent austral summers. We find that there is a distinct tendency for the PL/TDW and diurnal tide to be anticorrelated. When a well-defined PL/TDW exists, the diurnal tide is virtually nonexistent. This behavior is most striking at Darwin

for2013 (the longest continuous set of wind data we analyzed). The data shown in Figure 10 showed a clear TDW signature and a strong diurnal tide. The main feature occurred in mid-January had a period close to 48 h and attained an amplitude of ~45 m/s. The event was preceded and followed by a diurnal tide, with the virtual absence of a tide during the event. A second weaker TDW event (~30 m/s) had a period very close to 48 h. During the event there was a substantial decrease in the diurnal tide (diminishing from ~70 m/s to 40 m/s). This appearance of this event in the data is very striking. As this PL/TDW event diminished, the diurnal tide recovered to previous amplitudes. Other examples are shown in the earlier study [*Hecht et al*., 2010]. The results of an analysis of MF radar data from BP for January 2003 are particularly striking, with nearly a factor of 5 increase in the amplitude of the diurnal tide as a PL/TDW event abates. As discussed in the section 1, the behavior of the TDW and tide are consistent with a PSI mechanism transferring energy from the tide to a TDW that is resonant at close to a diurnal subharmonic period.

We note that while in most cases analyzed, the peak power occurs at periods very close to 48 h, there are a few instances when the peak power occurs after the frequency of the peak has migrated to significantly higher or lower values (see Figures 2, 5, and 12). In one case (Figure 12) the peak period seen in the winds at one location (BP) differs from the periods very close to 48 h seen at all other locations at the same time and in the airglow data from the same time at BP. It is possible that in the other cases the wave continues to be accelerated by an off-resonance PSI as the period slowly drifts away from the subharmonic frequency [*McEwan and Plumb*, 1977].

We do not claim that the TDW originates via interactions with the tide. We do claim that that the evidence favors the proposal that during a PL/TDW event a PSI accelerates a preexisting TDW whose natural frequency is close to the diurnal subharmonic frequency [*Salby*, 1981; *Hagan et al*., 1993]. We suggest that the Plumb mechanism [*Plumb*, 1983] provides the preexisting TDW and the background winds tune the real frequency of the TDW so that the band pass of the resonance includes the 48 h subharmonic frequency. Using a middle atmosphere model, *Pendlebury* [2012] found a correlation between the strength of the TDW and the strength of the mesospheric jet, with the period increasing as the mesospheric jet weakens. *McCormack et al*. [2010] found that there was a critical zonal wind speed at 80 km for the formation of a large amplitude DW6, and we suggest that this was also an indicator of the occurrence of resonance with the required tuning. *Limpasuvan and Wu* [2009] inferred from an examination of the structure of the TDW and its annual variations that the 2 day westward $s = 3$ wave exhibited dual characteristics of a normal mode and instability [*Salby*, 1981; *Plumb*, 1983].

An alternative to the PSI mechanism (or its relatives) for explaining the anticorrelation with the diurnal tide is that the TDW alters the background through which the tide must propagate, and the TDW is accelerated by other means (e.g., baroclinic instability [*Yue et al*., 2012]). This leaves an open question of why the acceleration should be greatest when the period is essentially 48 h or why the amplitude of the diurnal tide is not modulated at a 48 h period, as it clearly is not. A related possibility is that the background wind that promotes a baroclinic instability at precisely 48 h is also a background wind that could block the diurnal tide propagating up from below. This seems unreasonably fortuitous; moreover, the main diurnal mode is far from evanescence and its phase is speed much too fast to suffer significant attenuation related to Doppler effects. It is possible that the PL/TDW-tide anticorrelation is due to some other interaction between a PL/TDW and tide that scatters energy out of the diurnal tide that has not heretofore been considered (e.g., some form of mode coupling). The proposed mechanism along with alternatives should be addressed with mechanistic models where the normal-mode resonance of the background state might be tuned and detuned around 48 h [e.g., *Körnish and Becker*, 2010].

Finally, large spikes observed in the airglow brightness preceding a strong TDW event appear to be rather common. This may be caused by minor constituent transport induced by transience (a rapid amplitude increase in the TDW) as suggested previously by *Hecht et al*. [2010].

6. Conclusions

The wind and airglow data favor, on balance, the proposal that the summertime acceleration of the TDW in austral summer is a subharmonic resonance involving a TDW that has been tuned to a subharmonic period of the TDW [*Walterscheid and Vincent*, 1996; *Palo et al*., 1998, 1999; *Hecht et al*., 2010; *McCormack et al*., 2010]. The evidence supporting this is

1. The strongest TDW features have periods close to 48 h.
2. When the TDW period stabilizes near 48 h, the diurnal tide substantially weakens.
3. The coincidence at Adelaide (Buckland Park) and Cerro Pachon (Andes Lidar Observatory) is consistent with zonal wave number 3. This together with the 2 day periodicity is consistent with the 2 day normal mode.
4. The coincidence of the TDW acceleration and tidal acceleration/deceleration at all three sites widely separated in longitude and latitude indicates that the source of the behavior characterizing the events acts coherently on large scales.

Acknowledgments
Work at The Aerospace Corporation was supported by NSF grants AGS1042259 and AGS 1110206. The UIUC radar was supported by NSF grant AGS 1110334. The USU MTM measurements are supported by NSF grant AGS 0737698. The Buckland Park MF and Darwin meteor radars were supported by Australian Research Council grants DP0878144 and DP1096901. To request data not included herein, contact the lead author (Richard.Walterscheid@aero.org).

References

Allen, J. B. (1977), Short time spectral analysis, synthesis, and modification by discrete Fourier transform, *IEEE Trans. Acoust. Speech Signal Process.*, *ASSP-25*(3), 235–238.
Azeem, I. M. A., and S. E. Palo (2001), Eos Trans. AGU, 81(48), Fall Meet. Suppl., Abstract SA11A-16.
Azeem, S. M. I., S. E. Palo, D. L. Wu, and L. Froidevaux (2001), Observations of the 2-Day wave in UARS MLS temperature and ozone measurements, *Geophys. Res. Lett.*, *16*, 3147–3150, doi:10.1029/2001GL013119.
Craig, R. L., and W. G. Elford (1981), Observations of the quasi- 2-day wave near 90 km altitude at Adelaide (35°S), *J. Atmos. Sol. Terr. Phys.*, *43*, 1051–1056.
Franke, S. J., X. Chu, A. Z. Liu, and W. K. Hocking (2005), Comparison of meteor radar and Na Doppler lidar measurements of winds in the mesopause region above Maui, 758 Hawaii, *J. Geophys. Res.*, *110*, D09S02, doi:10.1029/2003JD004486.
Gelinas, L. J., J. H. Hecht, R. L. Walterscheid, R. G. Roble, and J. M. Woithe (2008), A seasonal study of mesospheric temperatures and emission intensities at Adelaide and Alice Springs, *J. Geophys. Res.*, *113*, A01304, doi:10.1029/2007JA012587.
Gu, S.-Y., T. Li, X. Dou, Q. Wu, M. G. Mlynczak, and J. M. Russell (2013), Observations of quasi-two-day wave by TIMED/SABER and TIMED/TIDI, *J. Geophys. Res. Atmos.*, *118*, 1624–1639, doi:10.1002/jgrd.50191.
Hagan, M. E., J. M. Forbes, and F. Vial (1993), A numerical investigation of the propagation of the quasi 2-day wave into the lower atmosphere, *J. Geophys. Res.*, *98*, 23,193–23,205, doi:10.1029/93JD02779.
Harris, T. J. (1994), A long term study of the quasi-two-day wave in the middle atmosphere, *J. Atmos. Sol. Terr. Phys.*, *56*, 569–579.
Harris, T. J., and R. A. Vincent (1993), The quasi-two-day wave observed in the equatorial middle atmosphere, *J. Geophys. Res.*, *98*, 10,481–10,490, doi:10.1029/93JD00380.
Hecht, J. H., R. L. Walterscheid, and M. N. Ross (1994), First measurements of the two-dimensional horizontal wavenumber spectrum from CCD images of the nightglow, *J. Geophys. Res.*, *99*, 11,449–11,460, doi:10.1029/94JA00584.
Hecht, J. H., R. L. Walterscheid, D. C. Fritts, J. R. Isler, D. C. Senft, C. S. Gardner, and S. J. Franke (1997), Wave breaking signatures in OH airglow and sodium densities and temperatures: 1. Airglow imaging, Na lidar, and MF radar observations, *J. Geophys. Res.*, *102*, 6655–6668, doi:10.1029/96JD02619.
Hecht, J. H., R. L. Walterscheid, and R. A. Vincent (2001), Airglow observations of dynamical (wind shear-induced) instabilities over Adelaide, Australia associated with atmospheric gravity waves, *J. Geophys. Res.*, *106*, 28,189–28,197, doi:10.1029/2001JD000419.
Hecht, J. H., S. Kovalam, P. T. May, G. Mills, R. A. Vincent, R. L. Walterscheid, and J. Woithe (2004), Airglow imager observations of atmospheric gravity waves at Alice Springs and Adelaide, Australia during the Darwin Area Wave Experiment (DAWEX), *J. Geophys. Res.*, *109*, D20S05, doi:10.1029/2004JD004697.
Hecht, J. H., A. Z. Liu, R. L. Walterscheid, and R. J. Rudy (2005), Maui Mesosphere and Lower Thermosphere (Maui MALT) observations of the evolution of Kelvin-Helmholtz billows formed near 86 km altitude, *J. Geophys. Res.*, *110*, D09S10, doi:10.1029/2003JD003908.
Hecht, J. H., R. L. Walterscheid, L. J. Gelinas, R. A. Vincent, I. M. Reid, and J. M. Woithe (2010), Observations of the phase-locked 2 day wave over the Australian sector using medium-frequency radar and airglow data, *J. Geophys. Res.*, *115*, D16115, doi:10.1029/2009JD013772.
Hickey, M. P., G. Schubert, and R. L. Walterscheid (1992), Seasonal and latitudinal variations of gravity wave-driven fluctuations in OH nightglow, *J. Geophys. Res.*, *97*, 14,911–14,922, doi:10.1029/92JA00795.
Holdsworth, D. A., and I. M. Reid (2004), The Buckland Park MF radar: Routine observation scheme and velocity comparisons, *Ann. Geophys.*, *22*, 3815–3828.
Holdsworth, D. A., I. M. Reid, and M. A. Cervera (2004), The Buckland Park all-sky interferometric meteor radar—Description and first results, *Radio Sci.*, *39*, RS5009, doi:10.1029/2003RS003014.
Huang, Y. Y., S. D. Zhang, F. Yi, C. M. Huang, K. M. Huang, Q. Gan, and Y. Gong (2013), Global climatological variability of quasi-two-day waves revealed by TIMED/SABER observations, *Ann. Geophys.*, *31*, 1061–1075, doi:10.5194/angeo-31-1061-2013.
Jacobsen, E., and R. Lyons (2003), The sliding DFT, *Signal Process. Mag.*, *20*, 74–80.
Körnish, H., and E. Becker (2010), A simple model for the interhemispheric coupling of the middle atmosphere circulation, *Adv. Space Res.*, *45*, 661–668, doi:10.1016/j.asr.2009.11.001.
Limpasuvan, V., and D. L. Wu (2009), Anomalous two day wave behavior during the 2006 austral summer, *Geophys. Res. Lett.*, *36*, L04807, doi:10.1029/2008GL036387.
LeBlond, P. H., and L. A. Mysak (1978), *Waves in the Ocean*, 602 pp., Elsevier Sci., New York.
McCormack, J. P., S. D. Eckermann, K. W. Hoppel, and R. A. Vincent (2010), Amplification of the quasi-two day wave through nonlinear interaction with the migrating diurnal tide, *Geophys. Res. Lett.*, *37*, L16810, doi:10.1029/2010GL043906.
McEwan, A. D., and R. A. Plumb (1977), Off-resonant amplification of finite internal wave packets, *Dyn. Atmos. Oceans*, *2*, 83–105.
McEwan, A. D., and R. M. Robinson (1975), Parametric instability of internal gravity waves, *J. Fluid Mech.*, *67*, 667–687.
Minorsky, N. (1982), *Nonlinear Oscillations*, 714 pp., Krieger, Melbourne, Fla.
Muller, H. G., and L. Nelson (1978), A traveling quasi 2-day wave in the meteor region, *J. Atmos. Sol. Terr. Phys.*, *40*, 761–766.
Palo, S. E., Y. I. Portnyagin, J. M. Forbes, N. A. Makarov, and E. G. Merzlyakov (1998), Transient eastward-propagating long-period waves observed over the South Pole, *Ann. Geophys.*, *16*, 1486–1500.
Palo, S. E., R. G. Roble, and M. E. Hagan (1999), Middle atmosphere effects of the quasi-two-day wave determined from a general circulation model, *Earth Planets Space*, *51*, 629–647.
Pendlebury, D. (2012), A simulation of the quasi-two-day wave and its effect on variability of summertime mesopause temperatures, *J. Atmos. Sol. Terr. Phys.*, *80*, 138–151, doi:10.1016/j.jastp.2012.01.006.

Pendleton, W. R., Jr., M. J. Taylor, and L. C. Gardner (2000), Terdiurnal oscillations in OH Meinel rotational temperatures for fall conditions at northern mid-latitude sites, *Geophys. Res. Lett.*, *27*(12), 1799–1802, doi:10.1029/2000GL003744.

Plumb, R. A. (1983), Baroclinic instability of the summer mesosphere: A mechanism for the quasi-two-day wave?, *J. Atmos. Sci.*, *40*, 262–270.

Poole, L. M. G. (1990), The characteristics of the mesospheric two-day wave as observed at Grahamstown (33.3°S, 26.5°E), *J. Atmos. Sol. Terr. Phys.*, *52*, 259–268.

Press, W. H., and G. B. Rybicki (1989), Fast algorithm for spectral analysis of unevenly sampled data, *Astrophys. J., Part 1*, *338*, 277–280.

Reid, I. M., B. G. W. Vandepeer, S. D. Dillon, and B. G. Fuller (1995), The new Adelaide MF Doppler radar, *Radio Sci.*, *30*, 1177–1189, doi:10.1029/95RS00731.

Ripa, P. (1981), On the theory of nonlinear wave-wave interactions among geophysical waves, *J. Fluid Mech.*, *103*, 87–115.

Salby, M. L. (1981), The two-day wave in the middle atmosphere: Observations and theory, *J. Geophys. Res.*, *86*(C10), 9654–9660, doi:10.1029/JC086iC10p09654.

Schubert, G., R. L. Walterscheid, and M. P. Hickey (1991), Gravity wave driven fluctuations in the OH nightglow from an extended, dissipative emission region, *J. Geophys. Res.*, *96*, 13,869–13,880, doi:10.1029/91JA00562.

Taylor, M. J., W. R. Pendleton Jr., C. S. Gardner, and R. J. States (1999), Comparison of terdiurnal tidal oscillations in mesospheric OH rotational temperature and Na lidar temperature measurements at mid-latitudes for fall/spring conditions, *Earth Planets Space*, *51*, 877–885.

Taylor, M. J., L. C. Gardner, and W. R. Pendleton Jr. (2001), Long period wave signatures in mesospheric OH Meinel (6,2) band intensity and rotational temperature at mid-latitudes, *Adv. Space Res.*, *27*(6–7), 1171–1179.

Torrance, C. T., and G. P. Compo (1998), A practical guide to wavelet analysis, *Bull. Am. Meteorol. Soc.*, *71*, 61–78.

Tunbridge, V. M., D. J. Sandford, and N. J. Mitchell (2011), Zonal wave numbers of the summertime 2 day planetary wave observed in the mesosphere by EOS Aura Microwave Limb Sounder, *J. Geophys. Res.*, *116*, D11103, doi:10.1029/2010JD014567.

Walterscheid, R. L., and G. G. Sivjee (1996), Very high frequency tides observed in the airglow over Eureka (80°N), *Geophys. Res. Lett.*, *23*, 3651–3654, doi:10.1029/96GL03482.

Walterscheid, R., and R. Vincent (1996), Tidal generation of the phase-locked 2-day wave in the Southern Hemisphere summer by wave-wave interactions, *J. Geophys. Res.*, *101*, 26,567–26,576, doi:10.1029/96JD02248.

Walterscheid, R. L., G. Schubert, and J. M. Straus (1987), A dynamical-chemical model of wave driven fluctuations in the OH nightglow, *J. Geophys. Res.*, *92*, 1241–1254, doi:10.1029/JA092iA02p01241.

Yeh, K. C., and C. H. Liu (1981), The instability of atmospheric gravity waves through wave-wave interactions, *J. Geophys. Res.*, *86*, 9722–9728, doi:10.1029/JC086iC10p09722.

Yue, J., H.-L. Liu, and L. C. Chang (2012), Numerical investigation of the quasi 2 day wave in the mesosphere and lower thermosphere, *J. Geophys. Res.*, *117*, D05111, doi:10.1029/2011JD016574.

Zhao, Y., M. J. Taylor, and X. Chu (2005), Comparison of simultaneous Na lidar and Mesospheric Temperature Mapper measurements and the effects of tides on the emission layer heights, *J. Geophys. Res.*, *110*, D09S07, doi:10.1029/2004JD005115.